Eur. Phys. J. D **38**, 47–57 (2006)
DOI: 10.1140/epjd/e2005-00324-1

THE EUROPEAN PHYSICAL JOURNAL D

Collision-energy-resolved Penning ionization electron spectroscopy of styrene, 2-vinylpyridine, and 4-vinylpyridine with He*(2^3S) metastable atoms

M. Yamazaki, N. Kishimoto, and K. Ohno[a]

Department of Chemistry, Graduate School of Science, Tohoku University, Aramaki, Aoba-ku, Sendai 980-8578, Japan

Received 28 October 2005
Published online 13 December 2005 –

Abstract. Collisional ionization of styrene (phenylethylene), 2-vinylpyridine, and 4-vinylpyridine with metastable He*(2^3S) atoms were studied by means of collision-energy/electron-energy resolved two-dimensional Penning ionization electron spectroscopy. Collision energy dependence of partial ionization cross-sections, which reflects the anisotropic interactions between a He*(2^3S) atom and the target molecules, indicates that attractive interaction for the out-of-plane access of a He*(2^3S) atom to phenyl group is stronger than that for the out-of-plane access to vinyl group. Moreover, it was found for vinylpyridines that the attractive interaction around π electrons became weaker than that for styrene, and that the attractive interaction for the in-plane access to the nitrogen atom is stronger than that for out-of-plane π-directions. However, in 2-vinylpyridine, the hydrogen atom of vinyl group prevents a He*(2^3S) atom from approaching to the nitrogen atom along in-plane directions, and thus the attractive interactions around the nitrogen atom were shielded by the vinyl group. The experimentally observed anisotropic interactions were qualitatively supported with ab initio model interaction potential calculations between a Li (He*(2^3S)) atom and the target molecule. Concerning with electronic structures of investigated molecules, the assignment of Penning ionization electron spectrum for 4-vinylpyridine was discussed on the basis of different behavior of collision-energy dependence of partial ionization cross-sections, and the satellite ionization band in Penning ionization electron spectra was also reported for styrene.

PACS. 34.20.Gj Intermolecular and atom-molecule potentials and forces – 34.20.Mq Potential energy surfaces for collisions – 34.50.Gb Electronic excitation and ionization of molecules; intermediate molecular states (including lifetimes, state mixing, etc.)

1 Introduction

Styrene (phenylethylene) and vinylpyridine are well known as one of the most typical materials in polymer chemistry. Their polymers are widely used for industrial and engineering applications, and the properties of the polymers and the interactions between aromatic π-systems and various materials have been extensively investigated in connection with physical, photochemical, and biological importance. On the more basic level, styrene and vinylpyridine are known as the simplest molecule in which an aromatic π ring is in conjugation with another unsaturated unit. The conjugation effect on both electronic structures and molecular structures of styrene and vinylpyridines has been studied by using various techniques, such as ultraviolet photoelectron spectroscopy [1–6], electronic absorption spectroscopy [7,8], and theoretical approaches [9–12]. Weakly bound clusters are utilized to study microscopic interaction of styrene with atoms [13] and molecules [14]. Resonant two-photon ionization spectra of styrene-water clusters were discussed by using a calculated structure of a styrene-water complex in which a water molecule lied above the styrene molecular plane with hydrogen bonds but was closer to the ethylene group than to the center of the benzene ring [14].

In π conjugated systems, there must be several interaction sites which produce local minima of an interaction potential energy surface. Although colliding beam experiments can give information on chemical reaction dynamics, it is in general not easy to elucidate anisotropy of intermolecular interactions. One of the experiments which combines the electron spectroscopy and the collision experiment is Penning ionization electron spectroscopy [15–18]. When a metastable atom A* collides with a target molecule M, where A* has an excitation energy larger than the lowest ionization potential (IP) of M, a chemi-ionization process known as Penning ionization [19] can occur:

$$A^* + M \rightarrow A + M_i^+ + e^-. \quad (1)$$

[a] e-mail: ohnok@qpcrkk.chem.tohoku.ac.jp

Based on the electron exchange model [20] proposed for the Penning ionization process, an electron in a molecular orbital (MO) of M is transferred to the inner-shell orbital of A* and the excited electron in A* is ejected. When a He*(2^3S) atom (the excitation energy, E(He*(2^3S)) = 19.82 eV) is used as A*, ionization into a final ionic state i takes place with a high probability when the $1s$ orbital of the He atom overlaps effectively with the target MO from which an electron is removed. Therefore, the reactivity of Penning ionization is directly related to the electron distribution of the ionized MO.

Penning ionization electron spectra (PIES), which is obtained from the analysis of ejected electron kinetic energy in Penning ionization, usually shows different band intensities, widths, and positions from those of ultraviolet photoelectron spectra (UPS). PIES contains the information on the orbital reactivity [21] for Penning ionization and on the anisotropic interactions between A* and M. Coupled experimental techniques including velocity (or collision energy) selection of He*(2^3S) atoms and electron kinetic energy analysis have been developed [22] to yield collision-energy/electron-energy resolved two-dimensional Penning ionization electron spectra (2D-PIES) [23]. Collision energy dependence of partial ionization cross-section (CEDPICS) obtained from 2D-PIES reflects the interactions around the regions where the ionized MO mainly extends, because the most reactive geometries for Penning ionization are governed by the electron distributions of the target MOs. Therefore, the 2D-PIES technique has been shown to be a powerful tool to investigate exterior characteristics of MOs and anisotropic interaction potential surfaces for various fundamental molecules with He*(2^3S) atoms [24]. For example, anisotropic interactions of He*(2^3S) with unsaturated compounds such as ethylenes [25–28], benzenes [25,29–32], and heterocyclic compounds [33] have been disclosed by 2D-PIES. Moreover, the different behaviour of CEDPICS for π and nitrogen lone-pair orbitals gave useful information on the assignments of PIES and UPS for azines [33]. Anisotropic interactions of molecules and the other metastable rare gas atoms (Rg*) such as He*($2\ ^1$S) [34], Ne* [35], and Ar* [36] have also been studied.

It is known that the shape of the velocity dependence of the total scattering cross-section of He*(2^3S) by He, Ar, and Kr is very similar to that of Li [37], and that the location of a interaction potential well and its depth are also very similar for He*(2^3S) and Li(2^2S) with various targets [38,39]. Although theory of Penning ionization for atomic targets has been established by Nakamura [40] and Miller [41], ab initio computational study on Penning ionization of molecular targets have been limited to simple molecules such as H_2 [42], N_2 [43], and H_2O [44] owing to the difficulty in obtaining anisotropic interaction potentials. The well-known similarity of a Rg* atom to a respective alkali atom [37–39] has therefore an advantage in estimation of anisotropic potentials, and have been successfully utilized to interpret the results of 2D-PIES for many molecules. Classical trajectory calculations on potential energy surface for N_2 and CH_3CN interacting with a Li atom well explained the experimental features of CEDPICS for He*(2^3S) + N_2 [45], CH_3CN [46]. The Li model potentials can also be modified in order to give quantitative agreement between experiments and calculations [30,47,48].

In this study, He*(2^3S) 2D-PIESs were measured for the phenyl and pyridyl substituted ethylenes (styrene, 2-vinylpyridine, and 4-vinylpyridine). Although ethylene [25,27] and substituted ethylenes [26,28] have been extensively studied by collision energy resolved measurements, it was difficult to evidently investigate the existence of weak attractive interactions with He*(2^3S) around π electron regions. However, it is possible to change the strength of interactions around vinyl π electron regions by a substitution of a π conjugation system for a hydrogen atom. Since a pyridine molecule strongly attract a He*(2^3S) atom at the directions where the lone pair electrons extend [33], it is also expected that vinylpyridines show different anisotropic interactions with He*(2^3S) from styrene. Moreover, the strength of attractive interactions around lone-pair electron regions is also changed by the vinyl substitution position of vinylpyridine owing to the steric effect of vinyl group in 2-vinylpyridine. From these points of view, the anisotropic interactions between a metastable helium atom He*(2^3S) and styrene, 2-vinylpyridine, and 4-vinylpyridine have been investigated by means of 2D-PIES combined with the Li model potential calculations in this study. The assignment of 2D-PIES for 4-vinylpyridine was also discussed on the basis of the slope of CEDPICS.

2 Experiment

The experimental apparatus used in the present study has been reported in previous papers [22,49]. He I ultraviolet photoelectron spectra (He I UPS) were measured by using the He I resonance photons (584 Å, 21.22 eV) produced by a discharge in pure helium gas. A metastable beam of He was produced by a nozzle discharge source, and the He*(2^1S) component was quenched by a water-cooled helium discharge lamp. The kinetic energy of electrons ejected during the Penning ionization or photoionization was measured by a hemispherical electrostatic deflection type analyzer using an electron collection angle 90° to the incident He*(2^3S) or photon beam. The transmission efficiency curve of the electron energy analyzer was determined by comparing our He I UPS data with those of Gardner and Samson [50] and Kimura et al. [4]. The energy resolution of the electron energy analyzer was 60 meV estimated from the full width at half maximum (*fwhm*) of the $Ar^+(^2P_{3/2})$ peak in the He I UPS. The background pressure in the reaction chamber was on the order of 10^{-7} Torr, and the experiments were performed under a sample pressure of ca. 2×10^{-5} Torr.

In collision-energy-resolved measurements, the metastable He*(2^3S) beam was modulated by a pseudorandom chopper [49] and then introduced into a collision cell located 504 mm downstream from the chopper disk. The

time-of-flight (TOF) of He* from the chopper to the collision cell can be obtained by the Hadamard transformation [49] of time-dependent electron signals emitted from a stainless steel plate inserted into the collision cell, since TOF of secondary electrons from the metal surface to the detector are negligibly short in comparison with that of the He* atoms. The time-dependent Penning ionization electron signals of sample molecules $I_e(E_e, t)$ as functions of electron kinetic energy E_e and time t were converted to $I_e(E_e, \tau_{TOF})$ as functions of E_e and TOF of the He* beam by the Hadamard transformation. The $I_e(E_e, \tau_{TOF})$ can be led to $I_e(E_e, v_{\mathrm{He}^*})$ as functions of E_e and velocity of He* atoms v_{He^*}. By the following equations, the 2D Penning ionization cross-section $\sigma(E_e, v_r)$ was obtained,

$$\sigma(E_e, v_r) = c\frac{I_e(E_e, v_{\mathrm{He}^*})}{I_{\mathrm{He}^*}(v_{\mathrm{He}^*})}\frac{v_{\mathrm{He}^*}}{v_r} \quad (2)$$

$$v_r = \sqrt{v_{\mathrm{He}^*}^2 + \frac{3k_BT}{m}} \quad (3)$$

where c is a constant, v_r is the relative velocity averaged over the velocity of the target molecule, k_B is the Boltzmann constant, and T and m are the gas temperature and the mass of the target molecule, respectively. The cross-section in equation (2) is normalized by using the velocity distribution of He* beam $I_{\mathrm{He}^*}(v_{\mathrm{He}^*})$. Finally, $\sigma(E_e, v_r)$ is converted to $\sigma(E_e, E_c)$ by the relation

$$E_c = \frac{1}{2}\mu v_r^2 \quad (4)$$

where μ is the reduced mass of the colliding system. Collision energy dependence of partial ionization cross-sections (CEDPICS) $\sigma(E_c)$ can be obtained by integrating 2D-PIES cross-sections $\sigma(E_e, E_c)$ over the E_e range related to each ionic state.

3 Calculations

All ab initio quantum chemical calculations were performed on the GAUSSIAN program [51]. It is generally difficult to obtain reliable interaction energies by the ab initio treatments of He*(2^3S) associated with highly excited electronic states embedded in ionization continua. Li(2^2S) has the same outer valence electronic configuration as He*(2^3S) with a $2s$ electron that mainly contributes to the interactions. For atomic targets (H, Li, Na, K, and Hg), quantitative estimation of the well depth of the Li model potential was recently summarized to be in good agreement with the ratio of 1.1 to 1.2 with respect to He*(2^3S) [39]. Based on the similarity between He*(2^3S) and Li(2^2S) [37–39], a ground state Li atom instead of a He*(2^3S) atom can be used to calculate the approximate potentials V_{Li} for V^*. The model interaction potential energy V_{Li} was obtained by the following manner

$$V_{\mathrm{Li}} = E_{\mathrm{MLi}} - (E_{\mathrm{M}} + E_{\mathrm{Li}}). \quad (5)$$

E_{MLi}, E_{M}, and E_{Li} are the total energy of the supermolecule (MLi), the isolated molecule (M), and the isolated Li atom, respectively. The Li model interaction potential calculations were performed by the second-order Møller-Plesset perturbation theory (MP2) with 6-311++G** basis set. The full counterpoise method [52] was employed to correct the basis set superposition error (BSSE). The molecular structures were fixed at the experimental or optimized equilibrium geometry. The geometry of a styrene molecule was selected from microwave spectroscopic measurements [53]. For 4-vinylpyridine and 2-vinylpyridine, the molecular structures were determined by the geometry optimizations at MP2 with 6-311++G** basis set.

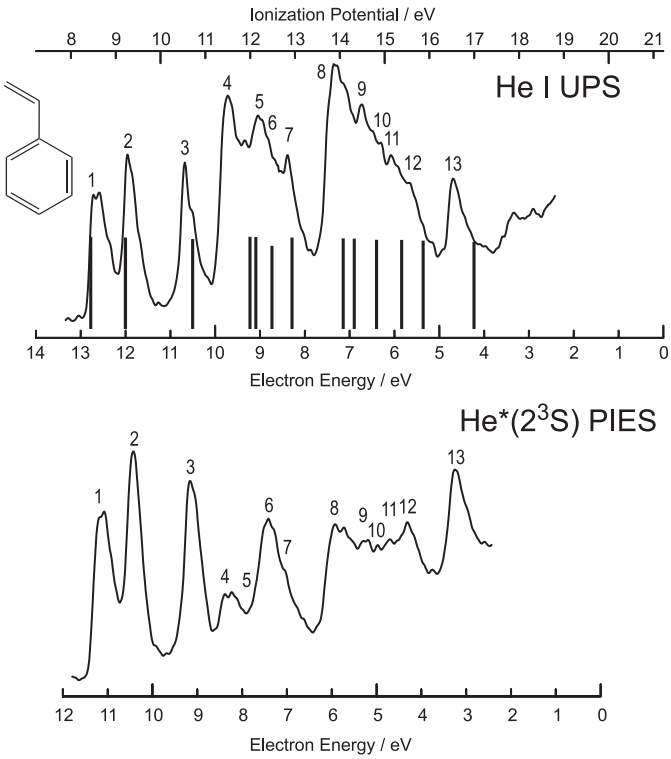

Fig. 1. He I UPS and He*(2^3S) PIES of styrene. Positions and heights of bar graphs in He I UPS show vertical ionization potentials and the pole strength by the OVGF method, respectively.

Vertical ionization potentials were calculated by using outer-valence Green's function (OVGF) [54] method with 6-311++G** basis sets in order to assign the ionic states of UPS and PIES. Electron distributions of molecular orbitals for the isolated target molecules were also obtained by ab initio self-consistent field (SCF) calculations using 6-311++G** basis sets.

4 Results

Figures 1–3 show He I UPS and He*(2^3S) PIES of the target molecules. The electron energy axes for PIES are shifted relative to those for the UPS by the difference in the excitation energies, 21.22 – 19.82 = 1.40 eV. Positions and heights of bar graphs in He I UPS show vertical ionization potentials (IP) and the pole strength by the OVGF method, respectively.

Table 1. Band assignments, observed ionization potential ($IP_{obs.}$), calculated ionization potential ($IP_{calc.}$), peak energy shift (ΔE), and obtained slope parameter (m) of the logσ–logE_c plots in CEDPICS for styrene, 2-vinylpyridine, and 4-vinylpyridine (see text).

molecule	band	orbital character	$IP_{obs.}$ / eV	$IP^{a}_{calc.}$ / eV	ΔE / meV	m
styrene	1	$4a''(\pi_4)$	8.50	8.44 (0.89)	−150	−0.34
	2	$3a''(\pi_3)$	9.26	9.21 (0.88)	−130	−0.36
	3	$2a''(\pi_2)$	10.54	10.71 (0.87)	−110	−0.29
	4	$24a'(\sigma)$	11.50	11.99 (0.89)	–	−0.13
	5	$23a'(\sigma)$	12.16	12.12 (0.88)	–	
	6	$1a''(\pi_1)$	(12.5)	12.48 (0.80)	–	−0.28
	7	$22a'(\sigma)$	12.84	12.93 (0.88)	–	
	8	$21a'(\sigma)$	13.86	14.07 (0.87)	–	−0.09
	9	$20a'(\sigma)$	14.48	14.32 (0.87)	–	
	10	$19a'(\sigma)$	14.92	14.82 (0.86)	70	
	11	$18a'(\sigma)$	15.14	15.38 (0.86)	–	
	12	$17a'(\sigma)$	15.54	15.86 (0.85)	–	
	S		(15.97)[b]			−0.22
	13	$16a'(\sigma)$	16.52	16.99 (0.84)	–	−0.15
2-vinylpyridine	1	$4a''(\pi_4)$	8.88	8.71 (0.89)	–	−0.34
	2	$24a'(n_N)$	9.52	9.71 (0.88)	−210	−0.33
	3	$3a''(\pi_3)$	10.24	10.14 (0.87)	–	−0.33
	4	$2a''(\pi_2)$	10.84	10.89 (0.87)	−70	−0.36
	5	$23a'(\sigma)$	12.10	12.38 (0.89)	–	−0.09
	6	$22a'(\sigma)$	12.78	13.20 (0.88)	–	
	7	$1a''(\pi_1)$	13.10	13.33 (0.80)	–	−0.29
	8	$21a'(\sigma)$	13.64	13.72 (0.87)	–	
	9	$20a'(\sigma)$	14.22	14.45 (0.87)	100	−0.15
	10	$19a'(\sigma)$	14.60	15.03 (0.86)	−130	
	11	$18a'(\sigma)$	15.52	15.75 (0.85)	–	
	12	$17a'(\sigma)$	15.94	16.26 (0.85)	–	
	13	$16a'(\sigma)$	16.68	17.10 (0.84)	–	−0.08
4-vinylpyridine	1	$4a''(\pi_4)$	9.23	9.21 (0.88)	(−60∼− 260)[c]	−0.25[d]
	2	$3a''(\pi_3)$	9.52	9.56 (0.88)	(−180∼− 380)[c]	
	3	$24a'(n_N)$	9.68	9.72 (0.87)	(−340∼− 580)[c]	−0.42[e]
	4	$2a''(\pi_2)$	11.36	11.55 (0.87)	−90	−0.27
	5	$23a'(\sigma)$	12.34	12.57 (0.89)	–	−0.08
	6	$22a'(\sigma)$	12.84	13.03 (0.88)	–	
	7	$1a''(\pi_1)$	13.14	13.28 (0.80)	–	−0.35
	8	$21a'(\sigma)$	14.14	14.37 (0.87)	–	−0.10
	9	$20a'(\sigma)$	14.30	14.57 (0.87)	–	
	10	$19a'(\sigma)$	14.94	15.16 (0.86)	–	
	11	$18a'(\sigma)$	15.47	15.91 (0.86)		
	12	$17a'(\sigma)$	16.03	16.40 (0.85)	–	
	13	$16a'(\sigma)$	16.65	17.09 (0.84)	−100	−0.12

[a]The pole strength in parenthesis. [b]Binding energy estimated from PIES. [c]Estimated from the plot of slope value of CEDPICS on electron energies in Figure 6a. [d]Estimated in the electron energy range from 10.0 to 10.8 eV. [e]Estimated in the electron energy range from 9.5 to 10.0 eV.

Table 1 lists the IP determined from the He I UPS and the assignment of the observed bands for styrene, 2-vinylpyridine, and 4-vinylpyridine. The assignments were determined based on the OVGF calculations and the IP values by the OVGF calculations are also shown in the table. The root mean square error between observed and calculated IPs was about 0.27 eV for all molecules. The pole strength for each ionic state was also shown in parentheses. The peak energy shifts (ΔE) in PIES measured with respect to the "nominal" energy E_0 (E_0 = the difference between the metastable excitation energy and the target IP) are also shown in the table. Values of the slope parameter m for the logσ vs. logE_c plots estimated by a linear least-squares method in a collision energy range from 90 meV to 280 meV are also listed in Table 1.

Figures 4–6 show (a) collision-energy-resolved PIES (CERPIES) and (b) CEDPICS obtained from the two-dimensional data of styrene, 2-vinylpyridine, and 4-vinylpyridine. The CERPIES are shown for low collision energy (ca. 92−111 meV), middle collision energy (ca. 134–169 meV), and high collision energy (ca. 207–279 meV). The CEDPICS were obtained by integrating electron counts of the 2D-PIES over an appropriate range of E_e and shown by the log σ vs. logE_c plots in

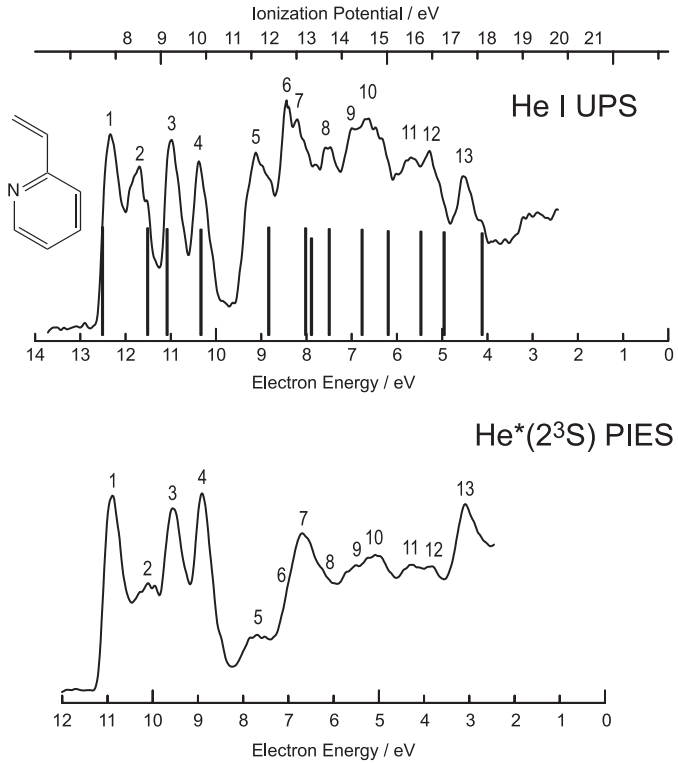

Fig. 2. He I UPS and He*(2^3S) PIES of 2-vinylpyridine. Positions and heights of bar graphs in He I UPS show vertical ionization potentials and the pole strength by the OVGF method, respectively.

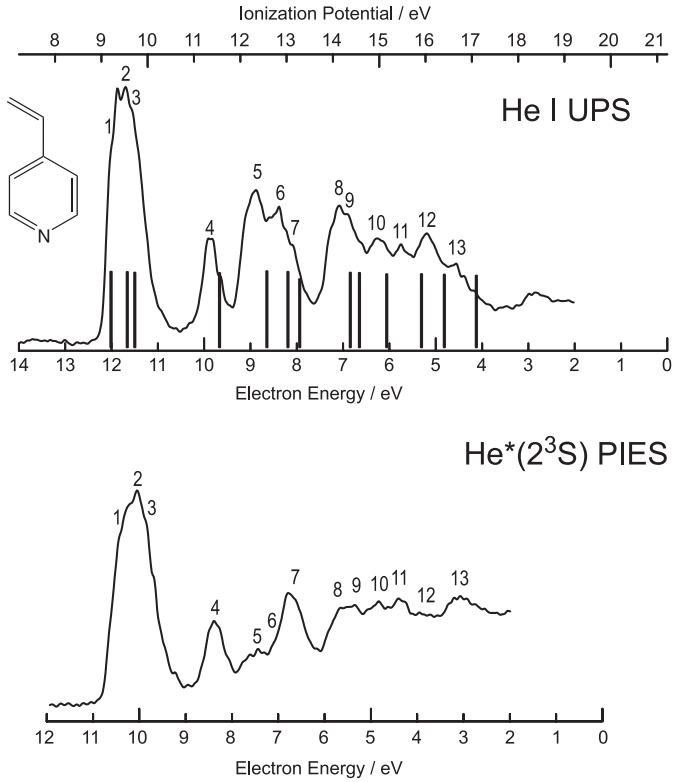

Fig. 3. He I UPS and He*(2^3S) PIES of 4-vinylpyridine. Positions and heights of bar graphs in He I UPS show vertical ionization potentials and the pole strength by the OVGF method, respectively.

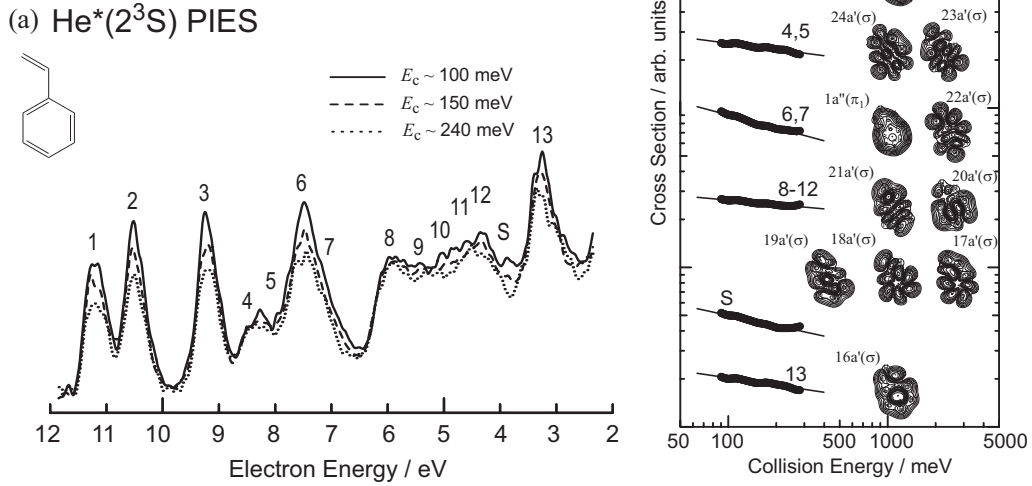

Fig. 4. (a) Collision-energy-resolved He*(2^3S) PIES of styrene; solid curve at 92–111 meV, average 100 meV; dashed curve at 134–169 meV, average 150 meV; dotted curve at 207–279 meV, average 240 meV. (b) Collision energy dependence of partial ionization cross-sections for styrene with He*(2^3S).

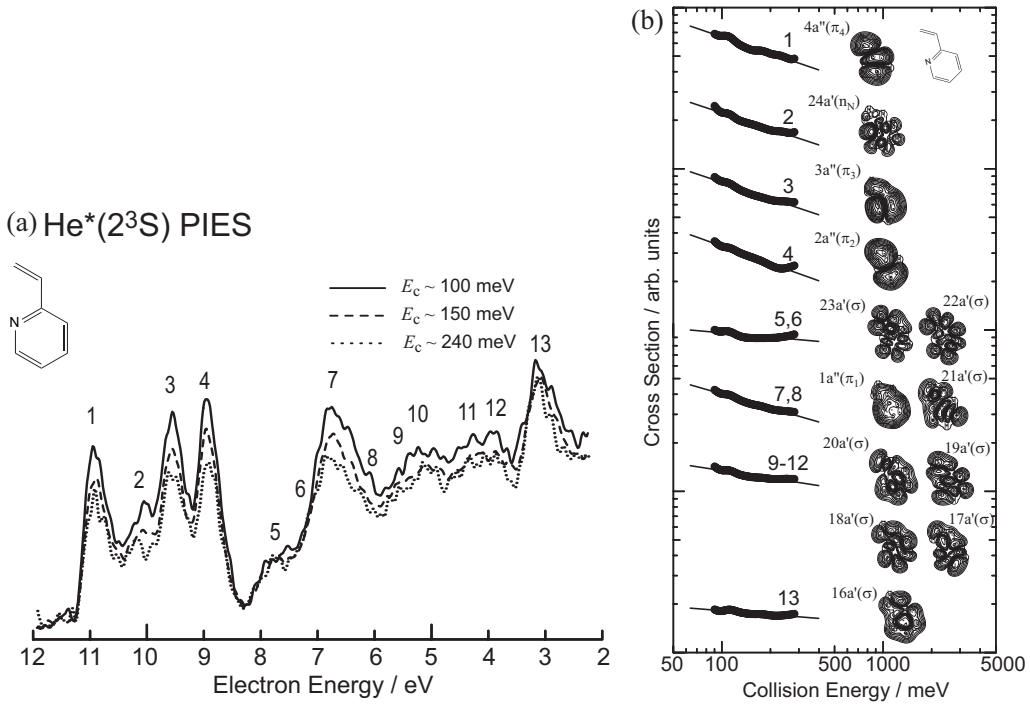

Fig. 5. (a) Collision-energy-resolved He*(2^3S) PIES of 2-vinylpyridine; solid curve at 92–111 meV, average 100 meV; dashed curve at 134–169 meV, average 150 meV; dotted curve at 207–279 meV, average 240 meV. (b) Collision energy dependence of partial ionization cross-sections for 2-vinylpyridine with He*(2^3S).

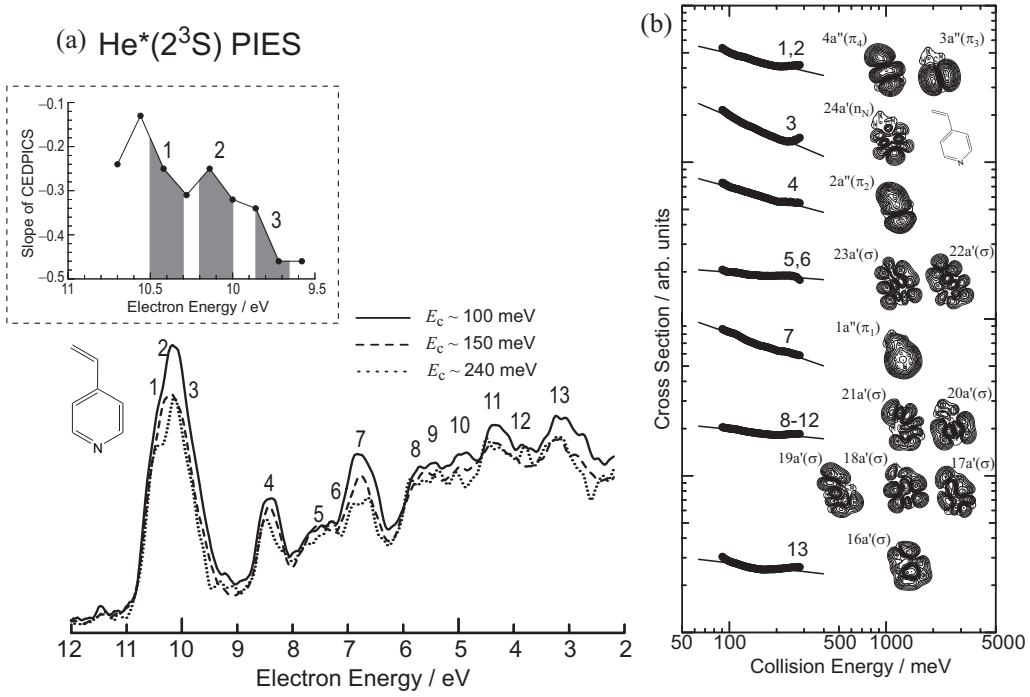

Fig. 6. (a) Collision-energy-resolved He*(2^3S) PIES of 4-vinylpyridine; solid curve at 91–109 meV, average 100 meV; dashed curve at 134–169 meV, average 150 meV; dotted curve at 209–282 meV, average 240 meV. Plot of slope value of CEDPICS for bands 1−3 at each electron energy with width of 140 meV is inserted. Band positions were roughly estimated as shown by shadings. (b) Collision energy dependence of partial ionization cross-sections for 4-vinylpyridine with He*(2^3S).

a collision energy range 90–280 meV. Thick solid lines in the CEDPICS indicate observed data and thin lines represent the least-squares-fitted lines. Electron density contour maps for respective molecular orbitals are also shown in Figures 4–6, in which the thick solid line in the maps represents the approximate molecular surface estimated from van der Waals radii of component atoms. The cutting planes of the electron densities are 1.0 Å away from the symmetry plane of each molecule. From the electron density maps, the effective access directions of a He* atom for the ionic state production can be known.

Figure 7 shows Li model potential curves of some selected directions for (a) styrene, (b) 2-vinylpyridine, and (c) 4-vinylpyridine. The distance R between Li and the molecule is measured from the centers of phenyl or vinyl group for out-of-plane access, and from the nitrogen atom for in-plane access to N atom.

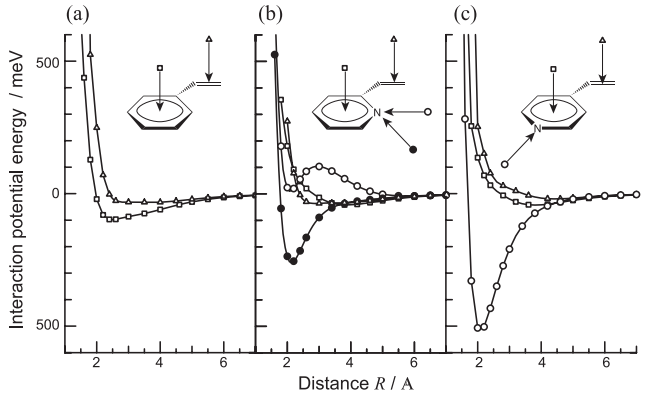

Fig. 7. Interaction potential energy curves for (a) styrene + Li, (b) 2-vinylpyridine + Li, and (c) 4-vinylpyridine + Li calculated at the level of MP2/6-311++G** with BSSE corrections: out-of-plane access to the phenyl group (square); out-of-plane access to the vinyl group (triangle); in-plane access to the N atom (circle); in-plane access to the N atom (filled circle).

5 Discussion

5.1 Styrene

The electronic interactions between the phenyl group and its substituents have been extensively studied by photoelectron spectroscopy [1]. The substitution of a hydrogen atom in benzene generally results in a lowering of the molecular symmetry and thus split the energy levels of highest occupied molecular orbitals (HOMO) in benzene depending on the electronic interaction between the phenyl group and the substituents. The conjugation effect between phenyl and unsaturated units causes electron delocalization and results in a splitting of energy levels for phenyl π orbitals. Styrene (phenylethylene) is known to show a strong conjugation effect, and the energy splitting of photoelectron bands in the low binding energy region of styrene has been well studied [2–5].

In Figure 1, bands 1, 2, 3, and 6 were assigned to the ionization from π orbitals that show strong band intensity in PIES [55]. It is of note that the $1a''(\pi_1)$ band (band 6) which is hidden under the three intense σ ionization bands in UPS is enhanced in PIES. This enhancement of π orbitals has also been observed in Ne* PIES of styrene [56]. Band 2 corresponds to almost pure $1e_{1g}(\pi)$ orbitals (HOMO) of benzene. However, one of the degenerate $1e_{1g}(\pi)$ orbitals of benzene interacts with the vinyl π orbital, and the resulting two MOs correspond to bands 1 and 3. Therefore the $4a''(\pi_4)$ and $2a''(\pi_2)$ orbitals are the destabilized phenyl π orbital and the stabilized vinyl π orbital, respectively. For the assignment of σ bands, the calculated IPs of $24a'(\sigma)$ and $23a'(\sigma)$ are very close to each other which is due to the degenerate $1e_{2g}(\sigma)$ orbitals of benzene. It is known that the degenerate $1e_{2g}(\sigma)$ orbitals of benzene are subject to pronounced interactions of the Jahn-Teller and pseudo Jahn-Teller types [57,58]. Band 13 has as large intensity as π bands, because the corresponding MO ($16a'$) is consist of in-phase combinations of all σ_{CH} units. This enhancement of σ_{CH} band intensities was also observed in the case of vinylpyridines in Figures 2 and 3 as well as in benzene [25,30,59] and pyridine [33]. In the case of styrene in Figure 1, band 12 was also observed to show relatively large intensity, which may be affected by the existence of additional satellite band and is mentioned later.

From the slopes m of CEDPICS in Table 1 and Figure 4, the anisotropic interactions between a styrene molecule and a He* (2^3S) atom can be studied. As discussed in previous papers [16,22,24], positive or negative slope of CEDPICS reflects the type of interaction between targets and He* atoms. In the case of attractive interaction, slower He* atoms can approach high electron density region more effectively due to a deflection of its trajectory. If a He* atom has enough speed to overcome attractive force, a He* atom and a target molecule cannot be close to each other effectively. Therefore, if the attractive interactions are dominant, CEDPICS shows a negative slope ($m < 0$). Niehaus [16] showed collision energy dependence of ionization cross-section for atomic targets by using classical relations. If the long-range attractive part of the interaction potential $V^*(R)$ plays a dominant role for collision dynamics, and its functional form is of the type

$$V^*(R) \propto R^{-s}, \tag{6}$$

energy dependence of the cross-section $\sigma(E_c)$ can be represented by

$$\sigma(E_c) \propto E_c^{-2/s}. \tag{7}$$

Therefore, the slope m of the logσ–logE_c plots can be related to the steepness of the attractive part of the interaction potential. In the case of repulsive interaction, on the other hand, faster He* atoms with high collision energy can approach reactive inner region of the target molecule, which results in positive CEDPICS ($m > 0$).

For styrene, the π bands show large negative slope ($m = -0.28 \sim -0.36$) of CEDPICS, which indicates that the interaction in the perpendicular region to the molecular plane is dominantly attractive. On the other hand, the slope values of CEDPICS for σ orbitals are relatively small ($m = -0.09 \sim -0.15$), and thus the ionization of σ orbitals should be affected by the repulsive interaction in the molecular plane. These experimental findings on anisotropic interactions can be supported by the Li model interaction calculations as shown in Figure 7. According to the Li model potentials, attractive interactions around the vinyl π orbital (the well depth $D \sim -30$ meV) are much weaker than those around phenyl π orbitals ($D \sim -100$ meV), which can be related to the fact that the stabilized vinyl π orbital, $2a''(\pi_2)$ shows weaker collision energy dependence ($m = -0.29$) than the destabilized phenyl π orbital, $4a''(\pi_4$, $m = -0.34$).

In CERPIES (Fig. 4), an additional band S observed around 3.85 eV in electron energy shows negative collision energy dependence. The slope of CEDPICS for the S band is –0.22 and is apparently different from those of σ orbitals. In PIES of He*(2^3S) + C_6H_6, the satellite bands have been observed [25,30,59]. The satellite bands can be interpreted to originate from the many-body

effect in ionization process. The S_1 band of He*(2^3S) + C_6H_6 around $E_e \sim 3.6$ eV was assigned to the ionization from the $1e_{1g}(\pi_2, \pi_3)$ orbitals (HOMO) associated with the $\pi(1e_{1g})-\pi^*(1e_{2u})$ excitation [59], since the binding energy for the S_1 band (16.1 eV) was in good agreement with the summation of the ionization potential (IP) corresponding to the $1e_{1g}(\pi_2, \pi_3)$ orbitals (9.25 eV) [4] plus the $\pi(1e_{1g})-\pi^*(1e_{2u})$ transition energy (6.95 eV) [60]. Green's function method [61] assigned the S_1 band to $^2A_{2u}$ state which originates from the interaction of the $1a_{2u}(\pi_1)$ hole and the $(1e_{1g})^{-2}(1e_{2u})^1$ configurations. Moreover, collision energy dependence of the S_1 band intensity showed negative slope [25,30], which supported the assignment based on the similarity in the slope of CEDPICS with the $1e_{1g}(\pi_2, \pi_3)$ orbitals (HOMO). Based on this fact, the S band in this study for styrene can be assigned to the satellite band that has relation with ionization from π orbitals.

5.2 2-vinylpyridine

In 2-vinylpyridine, the first four bands in UPS are well separated to each other. However, there must be the geometric isomers (rotational isomers) in 2-vinylpyridine according to the relative position of the CH_2 group to the N atom, which is characterized by the rotational angle ϕ around the CC single bond that connects the vinyl and the pyridine moieties. In this study, the trans-isomer with the CH_2 and the N atom to be most far apart from each other was defined to have the rotational angle $\phi = 180°$, and the other cis-isomer shown in Figures 2, 5, and 7 to have $\phi = 0°$. The existence of the geometric isomers should affect on both the intensity and its collision-energy dependence of 2D-PIES, although it was difficult to distinguish them in UPS. Ab initio calculations indicated that the difference in the electronic structures between the two isomers was very small. The OVGF calculation on the two isomers showed that the difference in IPs was at most 0.24 eV. From Figure 2, bands 1, 3, 4, and 7 are clearly assigned for the ionization from π orbitals because of their strong intensities in PIES, and the band 2 can be assigned to be the ionization from $24a'(n_N)$ orbital which is not conjugated with the vinyl π orbital. However, the intensity of n_N band is much weaker than those of π bands, whereas the n_N bands of azines showed as large intensities as π bands [33]. The relatively weak intensity of the n_N band in 2-vinylpyridine implies a steric hindrance for in-plane access of a He* atom to the N atom.

As the same case in styrene, the slopes of CEDPICS for the π orbitals are negatively larger than those for σ orbitals, which indicates that the interactions around π orbitals are more attractive. Concerning with the n_N band, it is well-known that the CEDPICS for an n_N band usually shows larger negative slope value than that for π bands as reported in previous studies on such as azines [33] and nitriles [49]. For example, the slope value of –0.54 was obtained for the CEDPICS of the ionization from the n_N orbital of pyridine [33], whereas those of π bands ranged from –0.34 to –0.49. However, no difference in the slope of CEDPICS for n_N band and π bands could be found in 2-vinylpyridine; the slope of CEDPICS for n_N band ($m = -0.33$) shows almost the same magnitude as those for π orbitals ($m = -0.29 \sim -0.36$). It must be noted here that the strength of the attractive interactions around the N atom does not become weak, and that the steric hindrance of the vinyl group causes relatively small slope value of CEDPICS for the n_N orbital of 2-vinylpyridine. The calculated model potential shown in Figure 7 clearly indicates the steric effect around the region where the n_N orbital extends. The Li model potentials shows repulsive potential energy for in-plane access to the N atom (open circles in Fig. 7b). When a Li atom approaches to the N atom in order to avoid the vinyl group (filled circles in Fig. 7b), the interaction potential became an attractive type one with a well depth of ca. 250 meV. In the case of the trans-isomer (trans-2-vinylpyridine) which has no steric effect of the vinyl group on the N atom, the Li model calculations showed that the interaction around the N atom became attractive type with the depth of 430 meV. Therefore, the vinyl group of cis-2-vinylpyridine shields the attraction of a He*(2^3S) atom to the N atom of cis-2-vinylpyridine. This is the reason because the negative energy dependence of the n_N band for 2-vinylpyridine is not as strong as those previously observed in nitrogen-containing compounds [33,49] and because the n_N band shows weaker intensity than π orbitals in PIES. As listed in Table 1, observed peak energy shift ($\Delta E = -210$ meV) for the n_N band of 2-vinylpyridine is comparable to the interaction well depth of ca. 250 meV, and is not so large compared with commonly observed ones (for example, the averaged ΔE for the n_N band of propionitrile, acrylonitrile, and 3-butenenitrile was ca. –340 meV [49]).

5.3 4-vinylpyridine

The UPS of 4-vinylpyridine has been already measured previously [6] in which three ionic states were observed in the binding energy region from ca. 8.5 eV to ca. 10.5 eV. Each ionic state is separated by a very small energy spacing of ca. 0.2 eV, which is caused by the interaction of π orbitals between subunits of a composite molecule. Concerning with the pyridine moiety, the first band of pyridine was carefully assigned to ionization from the lone-pair of nitrogen (n_N) by angle-resolved measurements of photoelectrons [62,63], multiphoton ionization spectroscopy [64], and PIES study [33], and the next-HOMO of pyridine is the $1a_2(\pi_3)$ orbital of which the N atom is on the nodal planes. However, the vinyl π orbital will not perturb the lone-pair ($11a_1(n_N)$) and π_3 ($1a_2$) orbitals of pyridine moiety, since the $11a_1$ and $1a_2$ orbitals cannot have significant overlap with the vinyl π orbital as shown in the electron density contour maps of 4-vinylpyridine (Fig. 6b). It is also noted that the IP value (9.68 eV) of the third ionic state of 4-vinylpyridine is very similar to that (9.67 eV) of the first ionic state of pyridine which corresponds to the ionization from the n_N orbital [33]. On the other hand, the $2b_1(\pi_2)$ orbital of pyridine can interact with the vinyl π orbital because of both the large overlap and the small energy

difference, which result in the $4a''(\pi_4$; HOMO) and the $2a''(\pi_2)$ orbitals of 4-vinylpyridine. A semi-empirical molecular orbital calculation (HAM/3) assigned the first three bands to be $4a''(\pi_4) < 24a'(n_N) < 3a''(\pi_3)$ in increasing order of IP [11]. On the other hand, OVGF AM1 calculations showed $4a''(\pi_4) < 3a''(\pi_3) < 24a'(\mathrm{n}_N)$ [12]. In this study, the OVGF calculation for 4-vinylpyridine resulted in nearly degenerate energy (the difference is 0.16 eV) for the second and the third ionic states which approximately corresponds to the ionization from $24a'(n_N)$ and $3a''(\pi_3)$ orbitals, respectively. Ortiz et al. pointed out [65] that the partial third order (P3) [54] and the OVGF method did not determine the order of the first two states for pyridine cation because the errors of these method with the cc-pVDZ basis were 0.19 and 0.25 eV, respectively, for typical molecules. In order to conclude the IP ordering of experimental energy spacing with ca. 0.15 eV, it is needed to apply more precise correlation methods and larger basis sets with an accuracy within 0.1 eV.

The largest negative slope value of CEDPICS should be found in bands 1–3, since the CEDPICS for an n_N band is usually different from those for π bands owing to the strong attractive interaction in the region where lone-pair electrons extend. Such kind of attractive interactions is caused by a dipole-induced dipole electrostatic attraction between a target molecule and a He* atom. For example, the slope value of CEDPICS for the lone-pair in an acetonitrile molecule was about two times larger than that for the π orbitals [46]. In the case of pyridine [33], the largest slope value of CEDPICS was also observed for the ionization from the n_N orbital as mentioned in Section 5.2. Actually, the Li model interaction calculation in Figure 7 showed the deepest point of the attractive interaction energy ($D \sim -500$ meV) in the direction where the lone-pair electrons of nitrogen extend (marked with circle in Fig. 7c). The change of slope values of CEDPICS for bands 1−3 on electron energy can be seen in the inserted graph in Figure 6a. A considerable change of the slope values was observed in the electron energy region from 9.72 to 9.86 eV. The largest negative slope (–0.46) of CEDPICS for bands 1–3 is found in the lower electron energy region, which suggest the existence of the ionic state related to the ionization from the $24a'(n_N)$ orbital. It is of note that, in the case of pyridine, the n_N band appeared in the second band of 2D-PIES, whereas the n_N band is the first ionic state in UPS. Moreover, the slope values for higher electron energy region are ranged from –0.13 to –0.34 (average −0.26) which are comparable to the slope value (−0.27) for the isolated band $4(\pi_2)$. In the case of 2D-PIES for 4-vinylpyridine, the assignments of bands 1–3 are thus $4a''(\pi_4) < 3a''(\pi_3) < 24a'(n_N)$.

The change of slope values of CEDPICS at each electron energy is due to the fact that the peak positions in PIES are usually shifted to higher or lower electron energy side with respect to the "nominal" energy E_0 (E_0 = the difference between the metastable excitation energy and the target IP). The energy of an electron ejected in Penning ionization is determined by the energy difference of entrance (M + He*(2^3S)) and exit (M_i^+ + He) channels. If the potential energy in exit channel is assumed to be nearly zero at the geometry where the ionization occurs, the peak energy shift ΔE will reflect the interaction energy in the entrance channel. Since the entrance potential energy surface exists above the exit one, the attractive interaction between the molecules and He*(2^3S) often cause a negative ΔE. In PIES of 4-vinylpyridine, the band corresponding to the electron removal from the lone-pair of nitrogen $24a'(n_N)$ is expected to show a large negative peak shift owing to the strong attractive interactions around nitrogen atom. If the third ionic state in UPS is assigned to be the $24a'(n_N)$ orbitals, ΔE for the electron energy region from 9.72 to 9.86 eV in PIES was from –580 meV to –340 meV which can be comparable to the well depth of 500 meV in the direction where the lone-pair of nitrogen extend as shown in Figure 7c. It is also of note that the negative peak energy shift for ionization from n_N orbital of pyridine was assumed to be –500 meV, [33] which is a value consistent with ΔE for the n_N band of 4-vinylpyridine.

As is the same with the cases of styrene and 2-vinylpyridine, the difference of CEDPICS between σ and π bands reflects the anisotropy of the potential surface. The negative slopes for π orbitals are much larger than those of σ orbitals, which indicates that the attractive interactions are dominant in the perpendicular directions of the molecular plane and the interaction for in-plane directions of the molecule is repulsive. However, the negative slope values of CEDPICS for π bands of 4-vinylpyridine become smaller than those of styrene. The Li model potential calculation also show weaker attractive interaction ($D \sim -43$ meV) around phenyl π electron region of 4-vinylpyridine than that of styrene ($D \sim -100$ meV) as shown in Figure 7. This can be interpreted by the effect of HOMO levels on attractive interaction in Penning ionization. Yamakado et al. measured CEDPICSs for the ionization from π orbitals of substituted ethylenes (ethylene, vinyl chloride, propene, and methyl vinyl ether), and the direct correlation between the slope of CEDPICS and the calculated energy level of HOMO was found [28]. For substituted ethylenes, the strengths of attractive interaction around π electrons increase as the energy levels of the HOMOs become higher. Molecular orbitals in higher energy levels can effectively interact with the $2s$-$2p$ orbitals of He* to give attractive interactions more strongly. For styrene and vinylpyridine, the same situation can occur because the HOMO level of 4-vinylpyridine is lower than that of styrene. It is of note that the attractive interactions around π electrons of azines [33] are also weaker than those of benzene [30] based on a recent 2D-PIES study.

The difference between 4-vinylpyridine and 2-vinylpyridine in interactions with He*(2^3S) can be found in the interaction around the vinyl group. As can be seen in Figure 7, the attractive interactions around the vinyl group of 2-vinylpyridine are stronger than that of 4-vinylpyridine. This difference can result in a relatively large negative slopes of CEDPICS for π bands of 2-vinylpyridine than those of 4-vinylpyridine. It is noted that the attractive region around the N atom exists not

only in-plane directions but also out-of-plane directions where the vinyl π orbital is distributed in the cis-isomer of 2-vinylpyridine ($\phi = 0°$).

6 Conclusion

Anisotropic interactions of styrene (phenylethylene), 2-vinylpyridine, and 4-vinylpyridine with a metastable He*(2^3S) atom were investigated by collision-energy/electron-energy-resolved two-dimensional Penning ionization electron spectroscopy combined with ab initio model interaction potential calculations. Observed partial ionization cross-sections showed different collision energy dependence depending on the spatial region where the ionized orbital extends. From observed slopes in log-log plot of collision energy dependence of partial ionization cross-sections (CEDPICS), the following remarks can be addressed.

(1) The attractive interaction for the out-of-plane access of a He*(2^3S) atom to phenyl group is stronger than to vinyl group of styrene.
(2) The interaction around σ orbital regions is dominantly repulsive for all molecules except for the region where nitrogen lone pair electrons of vinylpyridines extend.
(3) In 2D-PIES of 2-vinylpyridine, the existence of the geometric isomers affects the slope of CEDPICS and the band intensity for the ionization from the n_N orbital because the vinyl group of the cis-isomer prevents a He*(2^3S) atom from approaching to the attractive regions around the nitrogen atom.
(4) The attractive interaction around the nitrogen atom should be stronger than that of π electron regions, and the interaction around π electrons became weaker in 4- and 2-vinylpyridines than in styrene. Therefore, the strongest attractive direction was changed from out-of-plane directions of a styrene molecule to in-plane directions of vinylpyridine molecules by the effect of lone-pair electrons of the N atom.

These experimental findings were well supported with ab initio model interaction potential calculations between a Li atom and the target molecule on the basis of the similarity between a He*(2^3S) atom and a Li(2^2S) atom.

Regarding the observed electron spectra of styrene and 4-vinylpyridine, two points can be addressed by 2D-PIES. The satellite band in 2D-PIES of styrene clearly showed negative collision energy dependence of ionization cross-section, and it was related to the ionization from π orbitals and a shake-up process as with the same case of benzene [25,30,59]. Although the ordering of energy levels for nearly degenerated nitrogen lone-pair and π_3 orbitals of 4-vinylpyridine was not clearly determined, the large negative slope of CEDPICS enables us to confirm that the ionization from lone-pair (n_N) orbital of nitrogen appears as the third band in 2D-PIES.

The present work was supported by a Grant-in-Aid for Scientific Research from the Japanese Ministry of Education, Culture, Sports, Science and Technology. M.Y. is supported by the Research Fellowship of the Japan Society for the Promotion of Science for Young Scientists.

References

1. J.W. Rabalais, *Principles of Ultraviolet Photoelectron Spectroscopy* (Wiley, New York, 1977)
2. J.W. Rabalais, R.J. Colton, J. Electron Spectrosc. Relat. Phenom. **1**, 83 (1972/73)
3. T. Kobayashi, K. Yokota, S. Nagakura, J. Electron Spectrosc. Relat. Phenom. **2**, 449 (1973)
4. K. Kimura, S. Katsumata, Y. Achiba, T. Yamazaki, S. Iwata, *Handbook of He I Photoelectron Spectra of Fundamental Organic Molecules* (Japan Scientific, Tokyo, 1981)
5. K. Kesper, N. Münzel, W. Pietzuch, H. Specht, A. Schweig, J. Mol. Struct. (Theochem) **200**, 375 (1989)
6. A. Modelli, G. Distefano, J. Electron Spectrosc. Relat. Phenom. **23**, 323 (1981)
7. P. Swiderek, M.-J. Fraser, M. Michaud, L. Sanche, J. Chem. Phys. **100**, 70 (1994)
8. J.W. Ribblett, D.R. Borst, D.W. Pratt, J. Chem. Phys. **111**, 8454 (1999)
9. M. Dierksen, S. Grimme, J. Chem. Phys. **120**, 3544 (2004)
10. J. Wan, H. Nakatsuji, Chem. Phys. **302**, 125 (2004)
11. V. Barone, N. Bianchi, F. Lelj, G. Abbate, N. Russo, J. Mol. Struct. (Theochem) **108**, 35 (1984)
12. D.K. Danovich, V.K. Turchaninov, V.G. Zakrzewski, J. Mol. Struct. (Theochem) **209**, 77 (1990)
13. D. Consalvo, A. van der Avoird, S. Piccirillo, M. Coreno, A. Giardini-Guidoni, A. Mele, M. Snels, J. Chem. Phys. **99**, 8398 (1993)
14. H. Mahmoud, I.N. Germanenko, Y. Ibrahim, M.S. El-Shall, Chem. Phys. Lett. **356**, 91 (2002)
15. V.J. Čermák, J. Chem. Phys. **44**, 3781 (1966)
16. A. Niehaus, Adv. Chem. Phys. **45**, 399 (1981)
17. A.J. Yencha, *Electron Spectroscopy: Theory, Technique, and Application*, edited by C.R. Brundle, A.D. Baker (Academic, New York, 1984), Vol. 5
18. P.E. Siska, Rev. Mod. Phys. **65**, 337 (1993)
19. F.M. Penning, Naturwissenschaften **15**, 818 (1927)
20. H. Hotop, A. Niehaus, Z. Phys. **228**, 68 (1969)
21. K. Ohno, H. Mutoh, Y. Harada, J. Am. Chem. Soc. **105**, 4555 (1983)
22. K. Ohno, T. Takami, K. Mitsuke, T. Ishida, J. Chem. Phys. **94**, 2675 (1991)
23. K. Ohno, H. Yamakado, T. Ogawa, T. Yamata, J. Chem. Phys. **105**, 7536 (1996)
24. K. Ohno, Bull. Chem. Soc. Jpn **77**, 887 (2004)
25. T. Takami, K. Ohno, J. Chem. Phys. **96**, 6523 (1992)
26. K. Ohno, N. Kishimoto, H. Yamakado, J. Phys. Chem. **99**, 9687 (1995)
27. K. Ohno, K. Okamura, H. Yamakado, S. Hoshino, T. Takami, M. Yamauchi, J. Phys. Chem. **99**, 14247 (1995)
28. H. Yamakado, K. Okamura, K. Ohshimo, N. Kishimoto, K. Ohno, Chem. Lett. **26**, 269 (1997)
29. T. Horio, R. Maruyama, N. Kishimoto, K. Ohno, Chem. Phys. Lett. **384**, 73 (2004)
30. M. Yamazaki, S. Maeda, N. Kishimoto, K. Ohno, J. Chem. Phys. **122**, 044303 (2005)
31. N. Kishimoto, M. Furuhashi, K. Ohno, J. Electron Spectrosc. Relat. Phenom. **113**, 35 (2000)

32. K. Imura, N. Kishimoto, K. Ohno, J. Phys. Chem. A **105**, 4189 (2001)
33. N. Kishimoto, K. Ohno, J. Phys. Chem. A **104**, 6940 (2000)
34. D.C. Dunlavy, P.E. Siska, J. Phys. Chem. **100**, 21 (1996)
35. M. Albertí, M. Lucas, B. Brunetti, F. Pirani, M. Stramaccia, M. Rosi, F. Vecchiocattivi, J. Phys. Chem. A **104**, 1405 (2000)
36. M. Yamato, H. Ohoyama, T. Kasai, J. Phys. Chem. A **105**, 2967 (2001)
37. E.W. Rothe, R.H. Neynaber, S. Trujillo, J. Chem. Phys. **42**, 3310 (1965)
38. H. Haberland, Y.T. Lee, P.E. Siska, Adv. Chem. Phys. **45**, 487 (1981)
39. H. Hotop, T.E. Roth, M.-W. Ruf, A.J. Yencha, Theor. Chem. Acc. **100**, 36 (1998)
40. H. Nakamura, J. Phys. Soc. Jpn **26**, 1473 (1969)
41. W.H. Miller, J. Chem. Phys. **52**, 3563 (1970)
42. J.S. Cohen, N.F. Lane, J. Chem. Phys. **66**, 586 (1977)
43. T. Ishida, K. Horime, J. Chem. Phys. **105**, 5380 (1996)
44. T. Ishida, J. Chem. Phys. **105**, 1392 (1996)
45. T. Ogawa, K. Ohno, J. Chem. Phys. **110**, 3773 (1999)
46. T. Ogawa, K. Ohno, J. Phys. Chem. A **103**, 9925 (1999)
47. N. Kishimoto, T. Horio, S. Maeda, K. Ohno, Chem. Phys. Lett. **379**, 332 (2003)
48. S. Maeda, M. Yamazaki, N. Kishimoto, K. Ohno, J. Chem. Phys. **120**, 781 (2004)
49. N. Kishimoto, J. Aizawa, H. Yamakado, K. Ohno, J. Phys. Chem. A **101**, 5038 (1997)
50. J.L. Gardner, J.A.R. Samson, J. Electron Spectrosc. Relat. Phenom. **8**, 469 (1976)
51. M.J. Frisch et al., *Gaussian 03*, Revision C.02 (Gaussian, Inc., Wallingford CT, 2004)
52. S.F. Boys, F. Bernardi, Mol. Phys. **19**, 553 (1970)
53. K. Kuchitsu, E. Hirota, T. Iijima, W.J. Lafferty, D.A. Ramsay, *Landolt-Börnstein*, New Series II/21, 407
54. J.V. Ortiz, J. Chem. Phys. **104**, 7599 (1996)
55. K. Ohno, S. Matsumoto, Y. Harada, J. Chem. Phys. **81**, 4447 (1984)
56. T. Munakata, K. Kuchitsu, Y. Harada, Chem. Phys. Lett. **64**, 409 (1979)
57. H. Köppel, L.S. Cederbaum, W. Domcke, J. Chem. Phys. **89**, 2023 (1988)
58. M.S. Deleuze, A.B. Trofimov, L.S. Cederbaum, J. Chem. Phys. **115**, 5859 (2001)
59. S. Masuda, M. Aoyama, K. Ohno, Y. Harada, Phys. Rev. Lett. **65**, 3257 (1990)
60. J.P. Doering, J. Chem. Phys. **51**, 2866 (1969)
61. H.-G. Weikert, L.S. Cederbaum, Chem. Phys. Lett. **237**, 1 (1995)
62. C. Utsunomiya, T. Kobayashi, S. Nagakura, Bull. Chem. Soc. Jpn **51**, 3482 (1978)
63. M.N. Piancastelli, P.R. Keller, J.W. Taylor, F.A. Grimm, T.A. Garlson, J. Am. Chem. Soc. **105**, 4235 (1983)
64. C.R. Brundle, M.B. Robin, N.A. Kuebler, J. Am. Chem. Soc. **94**, 1466 (1972)
65. J.V. Ortiz, V.G. Zakrzewski, J. Chem. Phys. **105**, 2762 (1996)